

# Observation of Self-Organised Criticality in an Ultracold Atomic Gas

S. Helmrich,<sup>1</sup> A. Arias,<sup>1,2</sup> G. Lohead,<sup>1,2</sup> M. Buchhold,<sup>3</sup> S. Diehl,<sup>4</sup> and S. Whitlock<sup>1,2,\*</sup>

<sup>1</sup>*Physikalisches Institut, Universität Heidelberg,  
Im Neuenheimer Feld 226, 69120 Heidelberg, Germany.*

<sup>2</sup>*IPCMS (UMR 7504) and ISIS (UMR 7006),  
University of Strasbourg and CNRS, 67000 Strasbourg, France*

<sup>3</sup>*Department of Physics and Institute for Quantum Information and Matter,  
California Institute of Technology, Pasadena, CA 91125, USA*

<sup>4</sup>*Institut für Theoretische Physik, Universität zu Köln, 50937 Cologne, Germany*

(Dated: December 24, 2021)

Self organisation provides an elegant explanation for how complex structures emerge and persist throughout nature and society. Surprisingly often, these self-organised structures are found to exhibit remarkably similar fractal-like or scale-invariant properties. While this is sometimes captured by simple models featuring a critical point as an attractor for the dynamics, the connection to real-world complex systems is exceptionally hard to test quantitatively. Here we present the experimental observation of self-organised criticality in the dynamics of a driven-dissipative gas of ultracold atoms and a first characterisation of its universal properties. We show that population decay is a crucial aspect of the nonlinear dynamics that drives the system to a stationary state that is largely independent of the initial conditions and exhibits scale invariance as well as a strong response to perturbations. This establishes a well-controlled platform for investigating self-organisation phenomena and non-equilibrium universality with unprecedented experimental access to the underlying microscopic details of the system.

Self-organised criticality (SOC) is a fascinating concept, first put forward by Bak, Tang and Wiesenfeld in 1987 as a way to explain the abundance of scale-invariant systems found in nature [1]. It is thought to underlie a wide range of complex dynamical phenomena, ranging from activity in electrical circuits and neural networks [2, 3], to the likelihood of avalanches and earthquakes [4] as well as how forest fires [5, 6], diseases [7] and even ideas spread [8]. However, despite the wide ranging fundamental and practical importance of the SOC phenomenon, much-needed clean experimental studies are hindered by numerous complexities concerning the relevant microscopic degrees of freedom [9–12] and even the simplest toy models (beyond mean field approximations) present serious challenges to theory [13–19].

The defining characteristic of SOC is the emergence of scale invariance (characterised by self-similarity and algebraic scaling of spatio-temporal correlations) *without* the need to fine tune any system parameters. This is in contrast to scale invariance more commonly encountered in equilibrium systems which requires precise tuning to reach the critical point of a phase transition. While SOC is the prime example of criticality without fine tuning, similar phenomena are also encountered in other contexts such as hydrodynamic long-time tails [20], the Kosterlitz-Thouless critical phase in two-dimensional quantum fluids [21, 22], and the transient dynamics of turbulent cascades in isolated systems [23, 24] [for recent

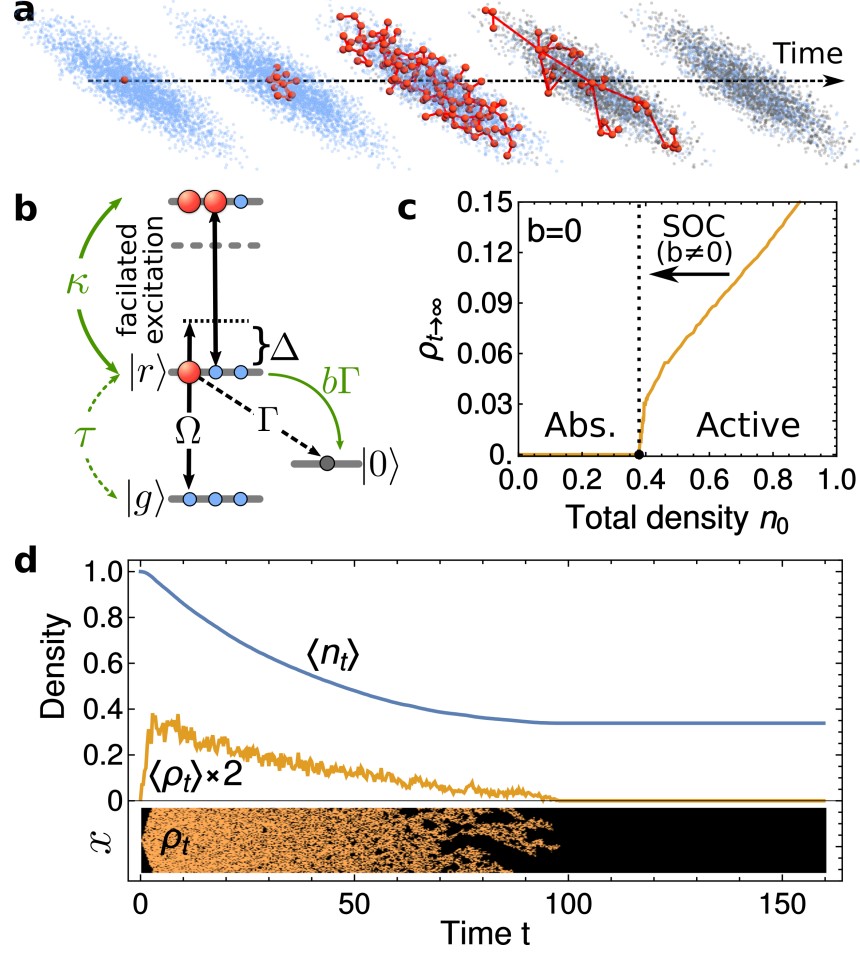


Figure 1. **Self-organised criticality in an ultracold atomic gas excited to Rydberg states by a laser field.** (a) Self-organisation process in a cigar shaped atom cloud showing atoms in the ground state  $|g\rangle$  (blue dots) or excited to a Rydberg state  $|r\rangle$  (large red spheres) via facilitated excitation processes leading to the build up of correlations (represented by red links). (b) The laser field couples the  $|g\rangle \rightarrow |r\rangle$  transition with Rabi frequency  $\Omega$  and detuning  $\Delta$  while atoms in the  $|r\rangle$  state either decay to removed states  $|0\rangle$  (black circles) or facilitate further Rydberg excitations. These microscopic processes determine the couplings in the Langevin equation (2) defined in the text (illustrated with green arrows and symbols). (c) Numerical solution of Eq. (2) for the population conserving system  $b = 0$  (in one-dimension) with  $D = 1$  (discretisation distance = 1),  $\Gamma = 10$ ,  $\kappa = 10$  and  $\tau = 0$ . As a function of the total density  $n_0$ , the stationary active density  $\rho_{t \rightarrow \infty}$  exhibits an absorbing state phase transition (dotted vertical line) which acts as an attractor for the SOC dynamics (when  $b \neq 0$ ). (d) Time evolution for  $b = 0.01$  showing the spatially-averaged active density  $\langle \rho_t \rangle$  (orange) and total density  $\langle n_t \rangle$  (blue) as the system approaches a stationary state close to the critical point of the absorbing state phase transition. The lower panel in (d) shows the full spatio-temporal evolution of the active density with transverse coordinate  $x$ .

studies involving ultracold atoms see Refs. [25, 26] (Kosterlitz-Thouless phase) and [27–29] (turbulence)]. In these examples however, scale invariance arises from an underlying symmetry or as a transient phenomenon rather than by dynamical self-tuning to a stationary critical point as in SOC.

We experimentally investigate the dynamics of a microscopically well-controlled physical system consisting of a three-dimensional gas of ultracold potassium atoms driven to highly excited Rydberg states by a laser field (Fig. 1a). As we will show, the crucial new ingredient leading to SOC is the irreversible decay of population to auxiliary inactive states, which has thus far been largely disregarded in the investigation of Rydberg many-body dynamics. This enables the observation of a phase transition from an absorbing to a self-organising active phase and universal scaling behavior without any fine-tuning. It also extends the application of ultracold Rydberg gases as widely tunable quantum many-body systems [30–35] to the study of self-organisation phenomena and universality in non-equilibrium dynamics.

Each of the  $1.3 \times 10^5$  atoms held in the optical trap can be represented by a three state system comprising: the ground state  $|g\rangle = |4s_{1/2}, F = 1\rangle$ , an excited Rydberg state  $|r\rangle = |39p_{3/2}\rangle$ , and auxiliary removed states, which we refer to collectively by  $|0\rangle$  (Fig. 1b). The laser field continuously drives the  $|g\rangle \rightarrow |r\rangle$  transition with a fixed detuning  $\Delta$  from resonance and with an amplitude parameterised by the Rabi frequency  $\Omega$ . In our experiments  $\Delta \gg \Omega$  such that spontaneous single-atom excitation processes are strongly suppressed. Once excited however, atoms can facilitate further excitations (e.g. when the laser detuning is compensated by the interaction energy of Rydberg pair states) leading to the formation of extended excitation clusters [36–45]. Alternatively, they can be spontaneously lost from the system, predominately by decaying to another hyperfine ground state that is not coupled by the lasers or to other states that are not optically trapped.

One major advantage of this system is that it permits an almost complete microscopic description in terms of a quantum master equation for the many-body density matrix  $\hat{\rho}$

$$\partial_t \hat{\rho} = \frac{i}{\hbar} [\hat{\rho}, \hat{H}] + \sum_l \mathcal{L}_l(\hat{\rho}) \quad (1)$$

with atom-light interaction Hamiltonian  $\hat{H}$  and Lindblad superoperator  $\mathcal{L}_l(\hat{\rho})$  given by

$$\begin{aligned} \hat{H} &= \sum_l \left[ \left( \sum_{\nu} \frac{1}{2} \frac{C_6}{|\mathbf{r}_{l\nu}|^6} \hat{\sigma}_{\nu}^{rr} - \Delta \right) \hat{\sigma}_l^{rr} + \frac{\Omega}{2} (\hat{\sigma}_l^{gr} + \hat{\sigma}_l^{rg}) \right], \\ \mathcal{L}_l(\hat{\rho}) &= \Gamma \hat{\sigma}_l^{0r} \hat{\rho} \hat{\sigma}_l^{r0} + \gamma_{\text{de}} \hat{\sigma}_l^{rr} \hat{\rho} \hat{\sigma}_l^{rr} - \frac{\gamma_{\text{de}} + \Gamma}{2} (\hat{\sigma}_l^{rr} \hat{\rho} + \hat{\rho} \hat{\sigma}_l^{rr}), \end{aligned}$$

where  $\hat{\sigma}_l^{\alpha\beta} \equiv |\alpha\rangle\langle\beta|_l$  and  $l, l'$  are indices for each atom. Interactions between Rydberg states are parameterised by the Van der Waals coefficient  $C_6/2\pi \approx 0.52 \text{ GHz } \mu\text{m}^6$  for the  $39p_{3/2}$  state. Dissipation is described by  $\mathcal{L}_l(\hat{\rho})$ , which includes spontaneous loss (with total rate  $\Gamma$ ) and irreversible dephasing (rate  $\gamma_{\text{de}}$ ) attributed primarily to residual laser phase noise and Doppler broadening.

For the system sizes explored in our experiment the quantum master equation (1) is computationally intractable and provides relatively little intuition. Thus we derive from it an effective coarse-grained description for the collective dynamics (Supplementary Information) which enables a direct comparison to known SOC models and access to controlled approximations. In brief, we average over the characteristic length scale corresponding to the facilitation process and project onto the density degree of freedom by adiabatically eliminating the rapidly decaying atomic coherences [46, 47]. We also approximate the atomic medium as a quasi-homogeneous gas with a smoothly varying density, which is justified by the fact that the atoms are free to move on the timescale of the SOC dynamics. The final result is a stochastic Langevin equation for the density of atoms in the  $|r\rangle$  state  $\rho_t = \rho(t, \mathbf{r})$  (which we call the active component) and the total remaining density  $n_t = n(t, \mathbf{r})$ , which is the sum of the populations in the  $|g\rangle$  and  $|r\rangle$  states (excluding removed states):

$$\begin{aligned}\partial_t \rho_t &= (D\nabla^2 - \Gamma + \kappa n_t)\rho_t - 2\kappa\rho_t^2 + \tau(n_t - 2\rho_t) + \xi_t, \\ n_t &= n_0 - b\Gamma \int_0^t dt' \rho_{t'}.\end{aligned}\tag{2}$$

In this equation  $D$  is the diffusion constant and  $\kappa$  is the facilitation rate which together govern the rate of excitation spreading,  $\tau$  is the spontaneous excitation rate,  $n_0$  is the initial density and  $b$  is a dimensionless parameter governing how fast decay depletes the total population. The stochastic part of the evolution is governed by the uncorrelated multiplicative noise term  $\xi_t = \xi(t, \mathbf{r})$  with variance  $\text{var}(\xi_t) = \Gamma\rho_t$ .

From equation (2) one can recognise all the key features of SOC. To illustrate this we present in Figs. 1(c,d) numerical simulations, for simplicity focusing on a small one-dimensional system. In the case: (i)  $b = \tau = 0$ , the system features a non-equilibrium phase transition [45] from an absorbing phase, where any excited component quickly dies out (characterised by  $\rho_{t \rightarrow \infty} \rightarrow 0$  for  $\kappa n_0 \ll \Gamma$ ), to an active phase in which excitations spread throughout the system from arbitrarily small seed excitations (with  $\rho_{t \rightarrow \infty} > 0$  for  $\kappa n_0 \gg \Gamma$ ). (ii) For  $b, \tau \neq 0$  on the other hand, spontaneous single-atom excitations trigger

the relatively fast facilitated excitation dynamics, while on longer timescales particle loss introduces a coupling between  $n_t$  and  $\rho_t$  giving rise to even richer non-Markovian evolution. Specifically, the integral in Eq. (2) acts as a feedback mechanism, causing  $n_t$  to continuously decrease while in the active phase. When this loss is slow compared to the internal dynamics but fast compared to the spontaneous excitation rate (achieved for  $\kappa n_0 \sim \Gamma \gg b\Gamma \gg \tau$ ), then the active density will develop growing spatio-temporal correlations until the dynamics terminate just below the critical point (as seen in the lower panel of Fig. 1d). (iii) In the limit  $D = \xi_t = 0$ , Eq.(2) coincides with the mean-field theory for the prototypical forest fire model for SOC [5]. The qualitative features of SOC can be understood from this minimalistic and easily tractable model, however the real experiment can be expected to show important quantitative differences that are captured only by the full Langevin equation (2). Importantly, the full dynamical many-body problem is remarkably difficult to solve theoretically, analytically or even numerically for large system sizes and in more than one spatial dimension [14, 16]. As a result, many properties of this system are still actively debated, such as the crucial question of whether the system self-organises towards a truly critical state, and whether it fulfils universal scaling relations expected for SOC [15, 18].

In particular, the non-equilibrium critical exponents for the model described by Eq. (2) have not been reliably determined beyond the mean field level. Limiting cases have been fully addressed, instead. For example, in the case that  $b = \tau = 0$  (number conserving and Markovian limit) the critical behaviour is governed by a critical point in the directed percolation universality class [17, 45]. How this universality changes in the non-commuting limit of  $b$  small but non-vanishing is not conclusively understood [15, 18], but we expect it to be strongly modified since, in a renormalisation group picture, the fully attractive SOC fixed point does not feature a relevant direction as is the case for directed percolation. In the non-interacting case  $\kappa = 0$ , the model features a Gaussian fixed point (with respect to  $\kappa$ ) in the dynamical percolation universality class [17]. However, this is presumably not smoothly connected to the Wilson-Fisher fixed point of the interacting non-Markovian problem. In what follows, we experimentally uncover universal properties of this elusive model, and provide a first experimental determination of one of its critical exponents.

Model verification – We start our experiments by investigating the full time evolution of the total remaining density for different initial states. For this we prepare a gas of atoms in the atomic ground state ( $\rho_0 = 0$ ) with different initial peak atomic densities  $n_0$

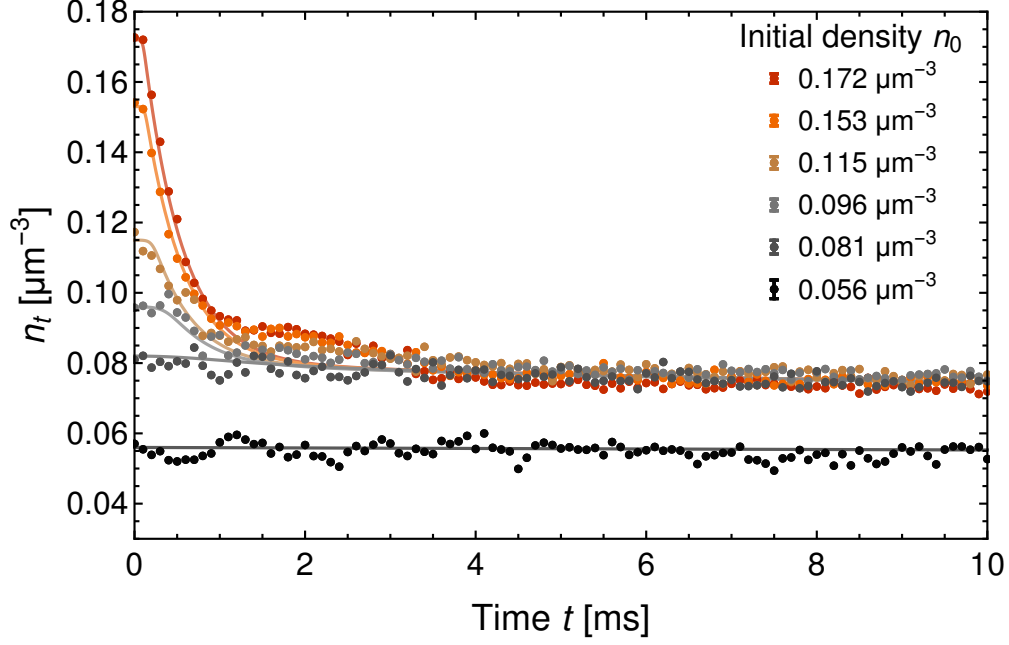


Figure 2. **Self-organisation:** Above a threshold value, the remaining total atom density  $n_t$  is attracted to the same stationary state density independent of the initial conditions. Parameters of the driving laser field are  $\Delta/2\pi = 30$  MHz,  $\Omega/2\pi = 190$  kHz. For high initial densities  $n_0 \gtrsim 0.08 \mu\text{m}^{-3}$  the time dependence consists of a short initial plateau followed by fast exponential decay to a unique stationary state with a fixed density  $n_f = 0.075 \mu\text{m}^{-3}$ . For initial densities below  $n_f$  the dynamics is frozen (black points). The solid lines correspond to mean field solutions to the effective Langevin equation with parameters given in the text. Standard errors for each dataset are indicated by the representative errorbars shown in the legend at top right.

between  $0.056(5) \mu\text{m}^{-3}$  and  $0.172(2) \mu\text{m}^{-3}$  where the numbers in parentheses refer to the standard error of the mean taken over several measurements. The Rydberg excitation laser is then suddenly switched on with constant  $\Omega/2\pi = 190$  kHz and  $\Delta/2\pi = 30$  MHz. After an adjustable time  $t$  we turn off the excitation laser and then take an absorption image of the remaining atoms to determine  $n_t$ . Fig. 2 shows that the time evolution of  $n_t$  is strikingly nonlinear, exhibiting two distinct types of behaviour depending on  $n_0$ . For high  $n_0$  it starts with a short initial plateau, followed by a rapid exponential decay, reflecting the initial growth of the excitation density followed by a high degree of activity. This decay finally cuts-off at a fixed density  $n_f = 0.075 \mu\text{m}^{-3}$  that is constant over a wide range of initial densities to a high accuracy (standard deviation of  $0.003 \mu\text{m}^{-3}$ ), indicating a stable

attractor for the many-body dynamics. In contrast, for  $n_0 < n_f$  the dynamics appears mostly frozen which is a consequence of the system remaining in the absorbing phase. These observations directly confirm the presence of the anticipated absorbing state phase transition and the self-organisation mechanism underlying the non-equilibrium evolution. On much longer timescales we observe a slower overall decay that we attribute to residual single atom excitations (and subsequent loss) with a characteristic rate  $\tau/2\pi = 1.12(2)$  Hz.

We now verify that the real system realizes the conditions for SOC, including the non-Markovian coupling between the active density and the total remaining density and the key hierarchy of scales  $\kappa n_0 \sim \Gamma \gg b\Gamma \gg \tau$ . For this it is sufficient to compare our data with a homogeneous mean field approximation to the Langevin equation ( $D = 0$  and  $\xi_t = 0$ ). We find that the mean field solutions, shown as solid lines in Fig. 2, describe the data well, except for the minor deviation in the approach to the stationary state seen around  $t \approx 2$  ms. By simultaneously fitting all of the data shown with a single set of parameters we find  $\Gamma/2\pi = 11.7(9)$  kHz,  $\kappa/2\pi = 144(10)$  kHz  $\mu\text{m}^3$  and  $b = 0.059(5)$ , with statistical errors estimated using bootstrap resampling. Thus the required separation of scales is satisfied by an order of magnitude or more, placing our experiments firmly in the interesting regime for SOC.

Phase transition and self-organised critical scaling – We now turn our attention to experimental manifestations of the observed phase transition and the critical nature of the stationary state. For this, the parameter  $\kappa$  is of special importance, since it determines the critical point of the absorbing state phase transition and its corresponding scaling behaviour. In our system  $\kappa$  is determined microscopically by the Rydberg excitation rate proportional to the driving intensity  $\Omega^2$  which can be tuned over a wide range. By comparing experimental timetraces for different detunings we additionally infer the relation  $\kappa \propto \Omega^2/\Delta^{2.06(1)}$ , which we use to compare the rest of the experimental results with theory without further free parameters. In Fig. 3 we examine the dependence of the stationary density  $n_f$  (reached after  $t = 10$  ms of evolution) on the driving intensity. For different initial densities  $n_0$ , the stationary state exhibits a clear density dependent critical intensity  $\Omega_c^2$  separating the absorbing phase (with  $n_f \approx n_0$ ) from the active self-organising phase (with  $n_f < n_0$ ). For the latter, the data falls onto a single curve resembling a power-law that is independent of the initial density (dotted blue line in Fig. 3a). While mean field theory (solid lines) reproduces the qualitative features of this data, the real, three dimensional system exhibits



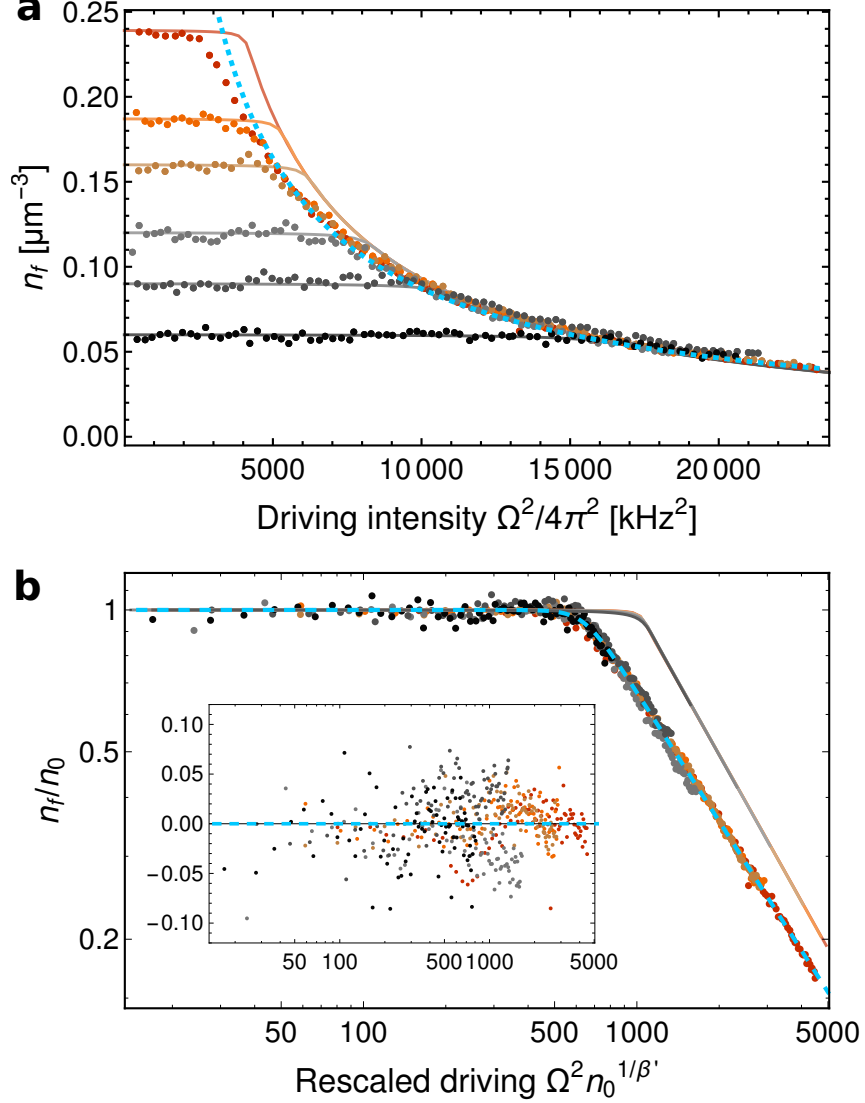


Figure 3. **Scale invariance of the self-organised stationary state as a function of the driving intensity  $\Omega^2$ .** (a) Stationary state density  $n_f$  measured at  $t = 10$  ms as a function of  $\Omega^2$  and for different initial densities  $n_0$  using the same parameters as for Fig. 2 except  $\Delta/2\pi = 18$  MHz. For large  $\Omega^2$  and  $n_0$  all points collapse onto one single powerlaw curve  $n_f \propto \Omega^{-2\beta}$  (dotted blue line). (b) The same data with rescaled axes to achieve full data collapse, revealing the universal scaling function (with fit shown by the dashed blue line) for the stationary density  $n_f$ . The inset shows the normalised residuals between the rescaled data and the fitted scaling function. Each datapoint is the mean of approximately 6 measurements. The solid lines in (a) and (b) correspond to mean field solutions of the effective Langevin equation.

important quantitative differences that go beyond the mean field prediction, including a shift in the threshold intensity seen for higher initial densities and a markedly different powerlaw exponent.

To further quantify the scale-invariant properties, we apply the scaling ansatz  $n_f = n_0 F(\Omega^2 n_0^{1/\beta'})$  [17]. By plotting  $n_f/n_0$  as a function of  $n_0^{1/\beta'} \Omega^2$ , all of the data collapse onto a single universal curve (Fig. 3b), with the best results obtained with a rescaling exponent  $\beta' = 0.869(6)$ . We find that the scaling function  $F(x)$  can be very well modelled by the heuristic function  $F(x) = x_c^\beta (x^{v\beta} + x_c^{v\beta})^{-1/v}$  (dashed blue curve in Fig. 3b), where  $x_c$  and  $v$  are free parameters describing the position and sharpness of the transition region between absorbing and active phases. For  $x \gg x_c$  the scaling ansatz is a powerlaw  $n_f \sim \Omega^{-2\beta} n_0^{1-\beta/\beta'}$ , therefore we identify  $\beta$  as the scaling exponent which characterises the stationary density and  $1 - \beta/\beta'$  quantifies how (in)sensitive it is to the initial density. Fitting the rescaled data on a log-log scale we obtain  $\beta = 0.910(4)$ ,  $v = 10.6(8)$  and  $x_c = 641(3) \text{ kHz}^2 \mu\text{m}^{-3/\beta'}$  where the small statistical errors of the fitted parameters are indicated in parentheses. Using these parameters, the scaling function describes the stationary density extremely well. This is confirmed by the small and evenly scattered normalised residuals between the rescaled data and the fitted scaling function, spanning both the absorbing and active phases (Fig. 3b-inset). Additional data taken under different experimental conditions confirms this measured scaling exponent within an accuracy of a few percent (Supplementary Information). In contrast, the mean-field scaling solution predicts  $\beta'_{MF} = \beta_{MF} = 1$ , which is clearly incompatible with our data. The fact that a single function, characterised by a non-trivial scaling exponent, describes the stationary state over the entire accessible parameter regime confirms that the SOC system does fulfil universal scaling and is a striking consequence of non-equilibrium universality going beyond mean field predictions.

Response to perturbations and avalanches – Having established the scale-invariant nature of the self-organised stationary state, we finally investigate its robustness to sudden perturbations. Assuming the critical state is indeed an attractor for the dynamics we expect that small perturbations, e.g. a sudden change of the spreading parameter  $\kappa$ , should trigger avalanche like processes that eventually bring the system back to a new critical state corresponding to a lower stationary density. On the other hand, if the system evolves to a state which is deep within the absorbing phase, then avalanches can only be triggered by perturbations larger than a threshold value, which we call the dynamical gap. To measure this response we

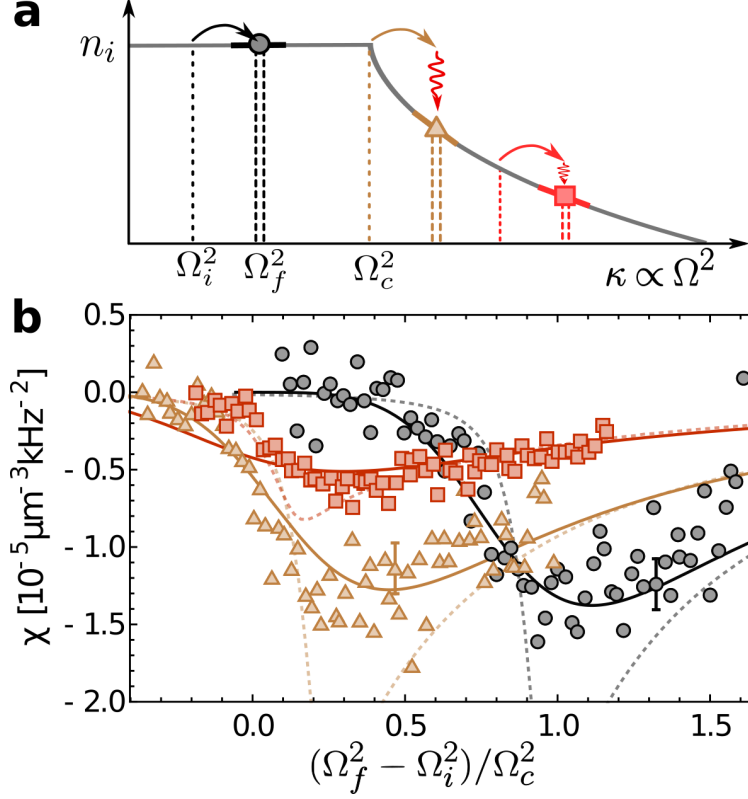


Figure 4. **Response of the self-organised critical state to external perturbations.** (a) Sketch of the experimental procedure used to measure the susceptibility  $\chi = dn_f/d(\Omega_f^2)$  by quenching the spreading parameter  $\kappa \propto \Omega^2$  across the absorbing state phase transition. (b) Experimental data corresponding to three different initial conditions corresponding to the absorbing phase (black circles), critical (brown triangles) and active phase (red squares). The solid lines correspond to predictions based on the experimentally determined scaling function and dotted lines correspond to mean field predictions. For reference we show two representative error bars corresponding to the standard error of the mean.

start from the stationary state (reached after  $t = 10$  ms) corresponding to different driving intensities  $\Omega_i^2$  (sketched in Fig. 4a). We then perturb the system by quenching the driving intensity to a new value  $\Omega_{f1}^2$  and then wait for a further 10 ms before measuring the new stationary density. The whole procedure is then repeated with a slightly larger final driving intensity  $\Omega_{f2}^2 \approx \Omega_{f1}^2 + (2\pi \times 50 \text{ kHz})^2$ . From these two measurements we estimate the susceptibility  $\chi = dn_f/d(\Omega_f^2) = [n_f(\Omega_{f1}^2) - n_f(\Omega_{f2}^2)]/(\Omega_{f1}^2 - \Omega_{f2}^2)$  where  $\Omega_f = (\Omega_{f1} + \Omega_{f2})/2$ .

Figure 4 shows the measured susceptibility as a function of  $\delta = (\Omega_f^2 - \Omega_i^2)/\Omega_c^2$  for three different initial conditions corresponding to  $\Omega_i < \Omega_c$  (absorbing),  $\Omega_i \approx \Omega_c$  (critical) and

$\Omega_i > \Omega_c$  (active). For each of these initial conditions we observe pronounced minima in  $\chi$  corresponding to the strongest system response. We interpret the leading edge on the left side of each minimum as the point where the perturbation is sufficient to bring the system back to the active phase, thereby triggering avalanche-like dynamics and extra loss. When starting deep in the absorbing phase (black circles) the onset occurs at a large value of  $\delta$ , which is a measure of the non-zero dynamical gap. In contrast, the onsets for critical (brown triangles) and active (red squares) initial states both coincide at  $\delta \approx 0$  within the experimental resolution. We can compare this data to a prediction of the susceptibility obtained from a derivative of the experimentally determined scaling function using  $\beta = 0.910$ . The scaling function predictions (solid lines in Figure 4) are in good agreement with the data, whereas mean field predictions (dotted lines) systematically fail to capture the widths and heights of the peaks. We note however that starting from the active initial state, the measured response is narrower and slightly stronger than the scaling function prediction. This indicates that, when starting deep in the active phase, the system does in fact self-organise to a well defined critical stationary state with a vanishing dynamical gap, rather than to a broad distribution of final states distributed around the critical point, irrespective of the precise value of  $\Omega_i > \Omega_c$ .

In this work we identified self-organised criticality as the underlying mechanism governing the complex dynamics of a driven open many-body system. Our main observations include a strikingly nonlinear evolution, a scale-invariant stationary state characterised by a non-trivial critical exponent  $\beta = 0.910(4)$  and a vanishing dynamical gap. The demonstrated versatility of ultracold Rydberg gases combined with the ability to understand and control the microscopic physics in this system almost completely, makes it a unique platform for studying non-equilibrium collective behaviour as it arises in diverse areas of physics. Future experiments may explore non-equilibrium dynamics governed by competing classical and quantum dynamical rules [48–50] and the interface between driven-dissipative and isolated quantum systems [27–29], ultimately leading to a comprehensive and quantitative understanding of non-equilibrium universality.

We acknowledge Thomas Ebbesen, Guido Pupillo and Matthias Weidemüller for discussions. This work is supported by the Deutsche Forschungsgemeinschaft under WH141/1-1 and is part of and supported by the DFG Collaborative Research Centre "SFB 1225 (ISOQUANT)", the Heidelberg Center for Quantum Dynamics, the European Union H2020 FET Proactive

project RySQ (grant N. 640378) and the ‘Investissements d’Avenir’ programme through the Excellence Initiative of the University of Strasbourg (IdEx). M. B. acknowledges support from the Alexander von Humboldt foundation. S.D. acknowledges support by the German Research Foundation (DFG) through the Institutional Strategy of the University of Cologne within the German Excellence Initiative (ZUK 81) and the European Research Council via ERC Grant Agreement n. 647434 (DOQS). S.W. was partially supported by the University of Strasbourg Institute for Advanced Study (USIAS), S.H. acknowledges support by the Carl-Zeiss foundation, A.A. and S.H. acknowledge support by the Heidelberg Graduate School for Fundamental Physics.

## METHODS

### A. Sample preparation

Our experiments are performed using a thermal gas of potassium-39 atoms, loaded directly from a magneto-optical trap (MOT) into a crossed optical dipole trap. The resulting cigar shaped atom cloud has a temperature of 40  $\mu\text{K}$  and  $e^{-1/2}$  radii of 10  $\mu\text{m}$  by 100  $\mu\text{m}$ . This should be compared to the characteristic distance between facilitated Rydberg excitations  $r_{\text{fac}} = (C_6/\Delta)^{1/6}$ , which for a detuning of  $\Delta/2\pi = 30 \text{ MHz}$  is  $\approx 1.7 \mu\text{m}$ . The peak number of atoms in the  $|g\rangle$  state is  $1.3 \times 10^5$  and the density determined by in-situ imaging is  $2.4 \times 10^{11} \text{ cm}^{-3}$ . To vary the density while holding all other parameters fixed we reduce the MOT loading time. The lifetime of the atoms in the trap without Rydberg excitation is  $\sim 4 \text{ s}$ , i.e. much longer than the relevant timescales for the SOC dynamics.

### B. Excitation laser

To excite the atoms to the  $39p_{3/2}$  Rydberg state we use a single photon optical transition at a wavelength of 285 nm. This light is produced by a frequency doubled dye laser delivering up to 200 mW of single mode light and is frequency stabilised to a high-finesse cavity resulting in an independently measured linewidth of 400 kHz. The excitation beam is aligned parallel to the long axis of the trap and weakly focused to a waist much larger than the size of the atom cloud such that it is practically uniform. We experimentally determine the Rabi frequency  $\Omega$  for every individual repetition of the experiment by logging the respective single-shot laser power on a photodiode and employing an independent Rabi frequency calibration based on

measuring light shifts induced by the laser via Ramsey interferometry.

### C. Numerical simulation of the Langevin equation

While the Langevin equation (2) is straightforward to solve in the mean field approximation, in Fig. 1 we show exemplary numerical simulations that capture the effects of diffusion and multiplicative noise terms in a one-dimensional setting. For these simulations we make use of the XMDS2 (stochastic) differential equation solver package [51], assuming a transverse grid size of 128 points and timestep of  $2.5 \times 10^{-3}$ . The noise term is implemented as a zero mean Wiener process with a standard deviation  $\propto \sqrt{\rho}$ . However, to ensure numerical stability we found it necessary to impose a noise cutoff by setting  $\xi = 0$  when  $\rho < 0.0025 n_0$ . For  $b = 0$  the solutions exhibit an absorbing state phase transition at  $n_0 = 0.39$  and powerlaw scaling consistent with directed percolation universality (in one-dimension  $\beta_{DP} = 0.276$ ). For  $b \neq 0$  we find that individual timetraces obtained from the full numerical solution are qualitatively very similar to the corresponding mean field solutions. By fitting the numerical results in the same manner as performed for the experimental data we obtain slightly larger effective parameters  $\kappa$  and  $\Gamma$ .

## SUPPLEMENTARY INFORMATION

### Derivation of the Langevin Equation

The microscopic dynamics of the driven-dissipative Rydberg ensemble is described by the master equation Eq. (1M). For realistic system sizes required for SOC, it becomes, however, intractable due to the fast growth of the Hilbert space. In order to reduce this theoretical complexity, we eliminate irrelevant degrees of freedom and map the dynamics to the Langevin equation Eq. (2M).

*Adiabatic elimination of atomic coherences* — In the presence of strong dephasing  $\gamma_{\text{de}} \gg \Omega$  the evolution of the atomic coherences  $\hat{\sigma}_l^{gr}, \hat{\sigma}_l^{0r}$  is dominated by a rapid dissipative decay towards their time averaged expectation values  $\langle \hat{\sigma}_l^{\alpha,r} \rangle_T = \frac{1}{T} \int_0^T \text{Tr} [\hat{\sigma}_l^{\alpha,r} \hat{\rho}] dt$ , where  $T \approx \Omega^{-1}$  is the typical time scale for a facilitated Rabi oscillation,  $\text{Tr}$  is the trace over the many-body Hilbert space and  $\alpha = g, 0$ . The coherences are static on many-body time scales and will be adiabatically eliminated by solving

$$0 \stackrel{!}{=} \partial_t \langle \hat{\sigma}_l^{\alpha,r} \rangle = \text{Tr} [\hat{\sigma}_l^{\alpha,r} \partial_t \hat{\rho}]. \quad (3)$$

Here  $\partial_t \hat{\rho}$  is set by Eq. (1M). After eliminating the coherences, the system evolution is governed by the remaining degrees of freedom, i.e. the average densities

$$m_l \equiv \text{Tr} [\hat{\sigma}_l^{rr} \hat{\rho}], \quad n_l \equiv \text{Tr} [(\hat{\sigma}_l^{rr} + \hat{\sigma}_l^{gg}) \hat{\rho}]. \quad (4)$$

Their equation of motion is

$$\partial_t m_l = \text{Tr} [\hat{\sigma}_l^{rr} \partial_t \hat{\rho}], \quad \partial_t n_l = \text{Tr} [(\hat{\sigma}_l^{rr} + \hat{\sigma}_l^{gg}) \partial_t \hat{\rho}] \quad (5)$$

and  $\partial_t \hat{\rho}$  is set by Eq. (1M) and constrained to configurations that fulfill Eq. (3). Explicit evaluation yields

$$\partial_t n_l = -\Gamma m_l + \xi_l^n, \quad (6)$$

$$\partial_t m_l = \text{Tr} \left( \frac{\Omega^2 (\Gamma + \gamma_{\text{de}}) (\hat{\sigma}_l^{gg} - \hat{\sigma}_l^{rr})}{(\Gamma + \gamma_{\text{de}})^2 + 4(\hat{V}_l - \Delta)^2} \hat{\rho} \right) - \Gamma m_l + \xi_l^m. \quad (7)$$

The Markovian noise fields  $\xi_l^{m,n}$  are added by hand in order ensure the non-equilibrium fluctuation-dissipation relation, present on the operator level, also on the level of the density averages (4). The statistics of  $n_l, m_l$ , imprinted by drive and dissipation, are expressed by the vanishing mean  $\langle \xi_l^{n,m} \rangle = 0$  and non-vanishing variance  $\text{var}(\xi_l^{n,m}) \neq 0$ , and the Markovianity,

i.e. locality in time and space, of the noise. Their variance is determined by the generalized Einstein relation

$$\begin{aligned}\text{var}(\xi_l^m) &= \partial_t \langle (\hat{\sigma}_l^{rr})^2 \rangle - 2 \langle \hat{\sigma}_l^{rr} \partial_t \hat{\sigma}_l^{rr} \rangle, \\ &= \tau n_l + (\Gamma + 2\tau) m_l + O(m_l^2),\end{aligned}\tag{8}$$

and similar for  $\xi_l^n$  with  $\hat{\sigma}_l^{rr} \rightarrow \hat{\sigma}_l^{rr} + \hat{\sigma}_l^{gg}$ . In the limit  $\tau \rightarrow 0$ , the variance of  $\xi_l^m$  is multiplicative in  $m_l$  which is a necessary condition for a robust absorbing phase.

Equation (7) is a coupled set of differential equations describing the Rydberg population and total remaining population for each atom, satisfying the completeness relation  $\hat{\sigma}_l^{rr} + \hat{\sigma}_l^{gg} + \hat{\sigma}_l^{00} = \mathbb{1}$ . Interatomic interactions enter as an effective detuning  $\hat{V}_l = C_6 \sum_{l' \neq l} \hat{\sigma}_{l'}^{rr} / |\mathbf{r}_{l,l'}|^6$ , where  $|\mathbf{r}_{l,l'}| = |\mathbf{r}_l - \mathbf{r}_{l'}|$  is the distance between atom  $l$  and  $l'$  [47].

In order to expand the trace in Eq. (7) in the projection operators  $\hat{\sigma}_{l'}^{rr}$ , one exploits the fact that  $\hat{\sigma}_{l'}^{rr} = (\hat{\sigma}_{l'}^{rr})^2$ . For an arbitrary function  $f$  of the projectors  $\hat{\sigma}_{l'}^{rr}$ , up to linear order in the projection operators one finds  $f(\{\hat{\sigma}_{l'}^{rr}\}) = f(0) + \sum_m [f(\hat{\sigma}_{l' \neq m}^{rr} = 0, \hat{\sigma}_m^{rr} = 1) - f(0)] \hat{\sigma}_m^{rr}$ . Consequently, the operator acting on atom  $l$

$$\begin{aligned}\frac{\Omega^2(\Gamma + \gamma_{\text{de}})}{(\Gamma + \gamma_{\text{de}})^2 + 4(\hat{V}_l - \Delta)^2} &= \underbrace{\frac{\Omega^2(\Gamma + \gamma_{\text{de}})}{(\Gamma + \gamma_{\text{de}})^2 + 4\Delta^2}}_{=\tau} + \\ &\sum_{l'} \left[ \frac{\Omega^2(\Gamma + \gamma_{\text{de}})}{(\Gamma + \gamma_{\text{de}})^2 + 4(\Delta - C_6 |\mathbf{r}_{l,l'}|^{-6})^2} - \tau \right] \hat{\sigma}_{l'}^{rr} + \dots,\end{aligned}\tag{9}$$

followed by higher order products of projectors (i.e. terms  $\sim \hat{\sigma}_{l'}^{rr} \hat{\sigma}_m^{rr}$ ). The first term on the right hand side describes single particle excitations with rate  $\tau$ , while the second term describe the facilitated (de-)excitation of atom  $l$  by another atom  $l'$  in the Rydberg state. This describes a Lorentzian peaked at the facilitation radius  $|\mathbf{r}_{l,l'}| = (C_6/\Delta)^{1/6} \equiv r_{\text{fac}}$  and deviates considerably from zero only for  $|\mathbf{r}_{l,l'}| \in [r_{\text{fac}} - \Delta r_{\text{fac}}, r_{\text{fac}} + \Delta r_{\text{fac}}]$  with  $\Delta r_{\text{fac}} = r_{\text{fac}} \frac{\Gamma + \gamma_{\text{de}}}{12\Delta}$ . Introducing a projector  $\Pi_{ll'}$  with  $\Pi_{ll'} = 1$  if  $|\mathbf{r}_{l,l'}| \in [r_{\text{fac}} - \Delta r_{\text{fac}}, r_{\text{fac}} + \Delta r_{\text{fac}}]$  and zero elsewhere, Eqs. (7)-(9) yield

$$\partial_t m_l = \left( \tau + \sum_{l'} \frac{\Omega^2 \Pi_{ll'} m_{l'}}{\Gamma + \gamma_{\text{de}}} \right) (n_l - 2m_l) - \Gamma m_l + \xi_l^m.\tag{10}$$

Equation (10) provides a good approximation to the facilitation rate assuming the excitation density is small, but overestimates the true facilitation rate when there is several Rydberg excitations in proximity to state  $l$  (due to truncating the expansion (9) at first order). An exact computation of the facilitation radius for  $w \geq 1$  excited states inside a



single shell shows that it grows as  $r_R^{(w)} = w^{1/6} r_R$  (in  $d = 3$  dimensions). For a homogenous distribution of atoms, this yields a facilitation rate that grows proportional to  $\sqrt{w}$ , which is not a severe correction compared to the  $\propto w$  growth predicted by Eq. (10) if one bears in mind the largely suppressed off-resonant excitation rate. Deviations from  $w = 0, 1$  are suppressed by a factor  $O(10^4)$ .

*Continuum Limit* — For the reported experiments the atoms are free to move on the timescale of the slow SOC dynamics. However, the diffusion time scale (set by the temperature) for distances of the order of the facilitation radius  $O(r_{\text{fac}})$  is about one order of magnitude slower than the inverse Rabi frequency. This justifies an effectively static model for the external degrees of freedom while ensuring that the the ground state density remains approximately homogenous on length scales compared to the facilitation radius. Thus we can coarse grain the dynamics by averaging the densities over facilitation shells

$$\rho(\mathbf{r}, t) \equiv \mathcal{N} \sum_{|\mathbf{r}_l - \mathbf{r}| \leq r_{\text{fac}}} m_l, \quad n(\mathbf{r}, t) \equiv \mathcal{N} \sum_{|\mathbf{r}_l - \mathbf{r}| \leq r_{\text{fac}}} n_l, \quad (11)$$

where  $\mathcal{N} = (\frac{4\pi}{3} r_{\text{fac}}^3)^{-1}$  is the normalization volume.

This coarse-graining procedure modifies the completeness relation compared to the single atom case. An excited atom facilitates excitations at the border of the facilitation shell but blocks the excitation for any atoms within the shell. Decay of a Rydberg excitation to a removed state thus removes the blockade constraint on the remaining ground state atoms. At the scale of the facilitation radius, the averaging procedure (11) yields the effective rate of decay into removed states is  $\Gamma \rightarrow b\Gamma$  and adds an effective decay rate back to the ground state  $\Gamma(1 - b)$ , where  $b = \rho(\mathbf{r}, t)/n(\mathbf{r}, t) \approx \text{const.}$  Defining  $n_t \equiv n(\mathbf{r}, t)$ ,  $\rho_t \equiv \rho(\mathbf{r}, t)$ , the averaged densities evolve as

$$\partial_t n_t = -b\Gamma \rho_t + \xi_t, \quad (12)$$

$$\partial_t \rho_t = -\Gamma \rho_t + \xi_t + (n_t - 2\rho_t) \left( \tau + \frac{\Omega^2}{\Gamma + \gamma_{\text{de}}} \mathcal{M}(\rho_t) \right). \quad (13)$$

The averaged noise  $\xi_t$  remains Markovian in time and space with variance  $\text{var}(\xi_t) = \tau n_t + (\Gamma + 2\tau)\rho_t$ . The nonlinearity  $\mathcal{M}(\rho_t)$  is obtained from the execution of the density averaging (11) in the sum  $\sim \sum_{l'} \Pi_{ll'} m_{l'}$  in Eq. (10). It is a non-local function in space and has to be read as  $\rho_t \mathcal{M}(\rho_t) = \rho(\mathbf{r}, t) \int_{\mathbf{r} - \mathbf{r}' \in S_{\text{fac}}} \rho(\mathbf{r}', t)$  with  $S_{\text{fac}} = [r_{\text{fac}} - \Delta r_{\text{fac}}, r_{\text{fac}} + \Delta r_{\text{fac}}]$  being the facilitation shell. Taking advantage of the smooth densities for  $|\mathbf{r}_{ll'}| = r_{\text{fac}}$  we can perform a

Taylor expansion of  $\rho(\mathbf{r}', t)$ , yielding

$$\mathcal{M}(\rho_t) = \mathcal{M}(1)\rho_t + \frac{\mathcal{M}(\mathbf{r}^2)}{2}\nabla^2\rho_t + O(\nabla^4\rho_t), \quad (14)$$

where odd derivative terms vanished due to isotropy in space. The factors  $\mathcal{M}(1) = \int_{\mathbf{r} \in S_{\text{fac}}} 1$  and  $\mathcal{M}(\mathbf{r}^2) = \int_{\mathbf{r} \in S_{\text{fac}}} \mathbf{r}^2$  are the averages of 1,  $\mathbf{r}^2$  along the facilitation shell.

Including thermal diffusion with diffusion constant  $D_T$  caused by the thermal motion of the atoms this yields the final form of the Langevin equation

$$\partial_t n_t = D_T \nabla^2 n_t - b\Gamma\rho_t + \xi_t, \quad (15)$$

$$\partial_t \rho_t = (D\nabla^2 + \kappa n_t - \Gamma - 2\tau)\rho_t - 2\kappa\rho_t^2 + \tau n_t + \xi_t. \quad (16)$$

In the experiment  $\Gamma/\tau \approx 10^4$  and  $n_t/\rho_t \approx 20$ , justifying to set  $\Gamma + 2\tau \rightarrow \Gamma$  and  $n_t + \rho_t \rightarrow n_t$ . Together with the numerical simulations this yields the estimate  $b \approx 0.05$ . Furthermore, the theoretical derivation predicts  $\kappa = \frac{\Omega^2}{\Gamma + \gamma_{\text{de}}} \mathcal{M}(1) \approx \frac{2\pi\Omega^2}{3\Delta} r_{\text{fac}}^3$  and  $D \approx D_T + n_t \frac{\pi\Omega^2}{3\Delta} r_{\text{fac}}^5$ . Assuming van der Waals interactions  $r_{\text{fac}} = (C_6/\Delta)^{1/6} \approx 1.7 \mu\text{m}$ . The diffusion of excitations  $\sim D$  is primarily governed by fast facilitation of neighboring atoms and only marginally affected by temperature, i.e.  $D_T \ll n_t \frac{\pi\Omega^2}{3\Delta} r_{\text{fac}}^5$ .

The structure of the Langevin equations (15), (16) is obtained from the discussed, controlled coarse graining procedure and is insensitive to minor variations of the microscopic details. The effective parameters  $D, \Gamma, \kappa, b, \tau$ , however, can be influenced by such variations, that may include disorder, atomic motion and cooperative excitation processes, in the present setup. For this reason, the predicted values above only serve as a rough guide and in order to compare theoretical predictions with the experimental results we fit the data to mean field solutions of Eq. (15) to consistently determine the relevant parameters of the model.

### Detuning dependence and further evidence for non-equilibrium universality

In the following we present additional evidence for the universal nature of the self-organised stationary state. For this we performed additional measurements of the stationary density as a function of the driving intensity but for different detunings of the excitation laser as shown in Fig. 5. Each dataset shows qualitatively similar behavior to that presented in Fig. 3, clearly showing the transition from an absorbing phase to a self-organising active phase. However this data also clearly shows that the location of the critical point depends on the laser detuning.

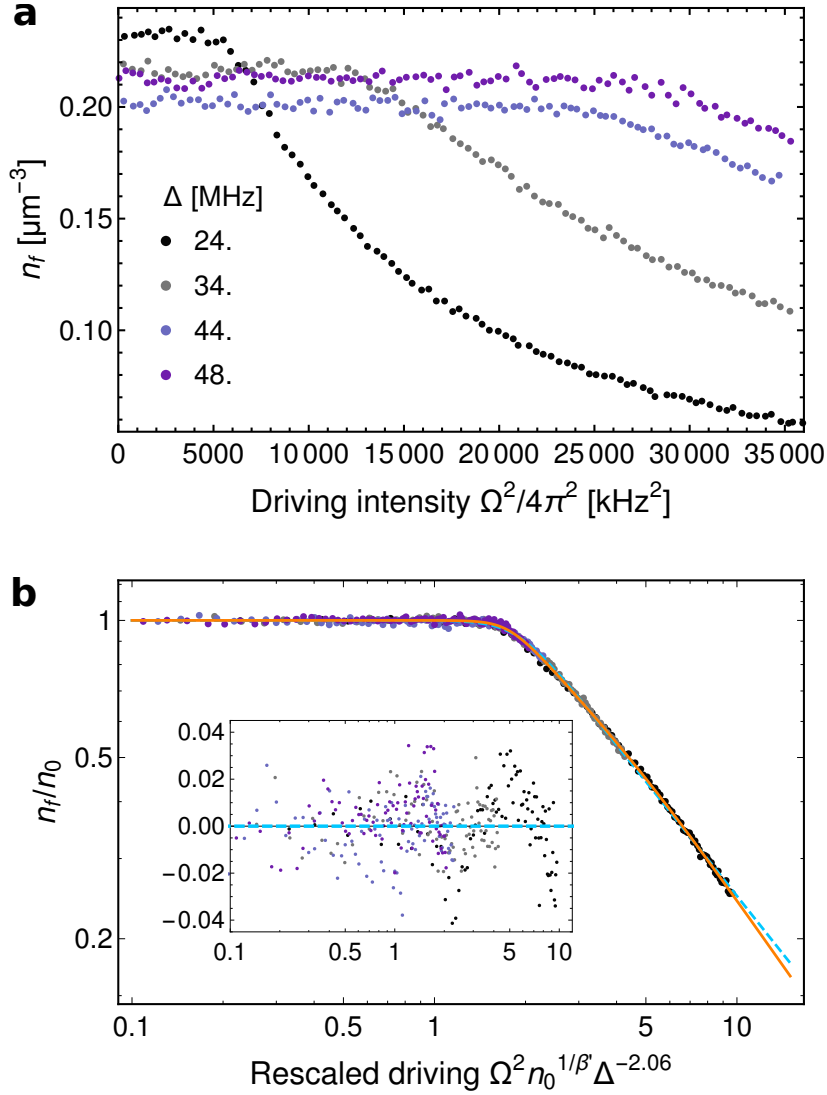


Figure 5. **Further evidence for non-equilibrium universality** (a) Stationary state density  $n_f$  measured at  $t = 10$  ms as a function of  $\Omega^2$  and for different detunings  $\Delta$ . (b) The same data with rescaled axes to achieve full data collapse, revealing the universal scaling function (with fit shown by the dashed blue line) for the stationary density  $n_f$ . The inset shows the normalised residuals between the rescaled data and the fitted scaling function. The dashed blue line corresponds to the simple scaling function used in the main text, while the solid orange line is a generalised scaling function which reproduces the asymptotic scaling form more accurately.

To further analyze this data we apply the scaling ansatz  $n_f = n_0 F(\Omega^2 \Delta^d n_0^{1/\beta'})$ , where  $\beta' = 0.869$  and we have included as a new parameter the detuning rescaling exponent  $d$ . For

$d = -2.06(1)$  the data collapses once again onto a single universal curve. In this way we determine the  $\kappa \propto \Omega^2/\Delta^{2.06}$  dependence of the spreading parameter, used elsewhere in the paper to compare the data with mean field theory.

Before analysing the scaling properties of the rescaled data, very careful inspection shows that it has a slightly different form to the scaling function  $F(x)$  used to describe the data in Fig. 3b. This is evidenced by the fit to  $F(x)$  shown as a blue dashed line in Fig. 5b. The deviation is most apparent in the normalized fit residuals (Fig. 5-inset) which, in contrast to Fig. 3b, exhibits some structure (e.g. the inverted U-shape of the black datapoints). Unless properly accounted for, this deviation between the scaling form of the data and the heuristic scaling function causes a systematic error in the determination of the critical scaling exponent. To rectify this, we model the detuning dependent data by a generalized scaling function  $F'(x) = [1 + (x/x_a)^{v\alpha} + (x/x_c)^{v\beta}]^{-1/v}$ , where the newly introduced parameters  $x_a < x_c$  and  $\alpha < \beta$  empirically describe power-law scaling for intermediate driving intensities. In the asymptotic regime  $x \gg x_c$ , the scaling function once again reduces to a power law  $n_f/n_0 \propto x^{-\beta}$ .

Fitting the generalized scaling function to the rescaled data yields  $\beta = 0.95(3)$  where the larger statistical uncertainty reflects the fact the generalized model function has more parameters. This is close to the value for  $\beta = 0.910(4)$  determined from the density dependent data in the main text. Refitting the density dependent data with the generalized scaling function yields  $\beta = 0.920(7)$ . This shows that, while the full form of the scaling function is not universal, data taken under very different conditions concerning initial densities and detuning of the driving field do in fact share a common universal critical exponent describing the asymptotic scaling regime.

We can also rule out possible modifications to the scaling behavior due to other experimental details such as the inhomogeneous density or residual effects of quantum coherence: (i) Inhomogeneities - in the experiment the atoms are laser-trapped in a cylindrical geometry of finite diameter and length, causing a nearly homogeneous density distribution in the trap center and smooth variation of  $n_t$  at the boundaries.  $n_t$  follows smoothly the Gaussian trapping profile of the lasers. To estimate the impact of inhomogeneities, on this basis we now study a local density approximation for the Langevin equation. In this approximation,  $\rho(\mathbf{r}, t)$  experiences a constant background density  $n(\mathbf{r}, t) = \tilde{n}(\mathbf{r}, t)I(\mathbf{r})$  at each point in space  $\mathbf{r}$ , which is modulated by the trapping profile  $I(\mathbf{r})$ , whereas  $\tilde{n}(\mathbf{r}, t)$  only incorpo-

rates fluctuations due to the coupling to  $\rho_t$ . An appropriate mean-field theory considers  $\rho_t = V^{-1} \int_V \rho(\mathbf{r}, t)$  as the spatially averaged density over the system volume  $V$  and  $\tilde{n}_{t=0} = n_0$  in the absence of fluctuations. The corresponding, spatially averaged SOC line is located at  $\Omega_c^2 \sim \kappa_c = \frac{\Gamma}{n_0} \int_V \frac{1}{I(\mathbf{r})} \sim n_0^{-1}$ , demonstrating that the mean-field exponent  $\beta = 1$  is not modified by the inhomogeneous geometry.

(ii) Quantum coherence - the evolution of the density averages (6), (7) is real and linear in time, which maps the final Langevin equation to a stochastic differential equation for classical processes. It incorporates strong, classical correlations between different atoms but lacks the possibility for long range coherence. Coherence between different atoms can be built in systematically by replacing the adiabatic elimination in Eq. (3) with the exact solution, which amounts to a shift  $\Gamma \rightarrow \Gamma + \partial_t$  in (7). To leading order it introduces a coherent contribution  $(\Gamma + \gamma_{\text{de}})^{-1} \partial_t^2 m_l$  to the RHS of (7). Analogously to a damped harmonic oscillator, this evolution is observable on timescales  $t(\Gamma + \gamma_{\text{de}}) \leq 1$  and washed out on larger times scales, i.e. on the relaxation towards the SOC steady state. Fast coherent processes might modify the parameters  $\kappa, D, \tau$  but not the structure of the Langevin equation.

---

\* e-mail: [whitlock@ipcms.unistra.fr](mailto:whitlock@ipcms.unistra.fr)

- [1] P. Bak, C. Tang, and K. Wiesenfeld, “Self-organized criticality: An explanation of the 1/f noise,” *Phys. Rev. Lett.* **59**, 381–384 (1987).
- [2] J. Hesse and T. Gross, “Self-organized criticality as a fundamental property of neural systems,” *Frontiers in Systems Neuroscience* **8**, 166 (2014).
- [3] W. L. Shew, W. P. Clawson, J. Pobst, Y. Karimipanah, N. C. Wright, and R. Wessel, “Adaptation to sensory input tunes visual cortex to criticality,” *Nature Physics* **11**, 659–663 (2015).
- [4] A. Sornette and D. Sornette, “Self-organized criticality and earthquakes,” *EPL (Europhysics Letters)* **9**, 197 (1989).
- [5] B. Drossel and F. Schwabl, “Self-organized critical forest-fire model,” *Phys. Rev. Lett.* **69**, 1629–1632 (1992).
- [6] B. D. Malamud, G. Morein, and D. L. Turcotte, “Forest fires: An example of self-organized critical behavior,” *Science* **281**, 1840–1842 (1998).

- [7] C. J. Rhodes and R. M. Anderson, “Power laws governing epidemics in isolated populations,” *Nature* **381**, 600–602 (1996).
- [8] J. P. Gleeson, J. A. Ward, K. P. O’Sullivan, and W. T. Lee, “Competition-induced criticality in a model of meme popularity,” *Phys. Rev. Lett.* **112**, 048701 (2014).
- [9] S. Field, J. Witt, F. Nori, and X. Ling, “Superconducting vortex avalanches,” *Phys. Rev. Lett.* **74**, 1206–1209 (1995).
- [10] V. Frette *et al.*, “Avalanche dynamics in a pile of rice,” *Nature* **379**, 49 (1996).
- [11] R. Dickman, M. A. Muñoz, A. Vespignani, and S. Zapperi, “Paths to self-organized criticality,” *Brazilian Journal of Physics* **30**, 27 – 41 (2000).
- [12] E. Altshuler and T. H. Johansen, “Colloquium: Experiments in vortex avalanches,” *Rev. Mod. Phys.* **76**, 471–487 (2004).
- [13] A. Vespignani and S. Zapperi, “Order parameter and scaling fields in self-organized criticality,” *Phys. Rev. Lett.* **78**, 4793–4796 (1997).
- [14] R. Dickman, “Numerical study of a field theory for directed percolation,” *Phys. Rev. E* **50**, 4404–4409 (1994).
- [15] M. A. Muñoz, G. Grinstein, R. Dickman, and R. Livi, “Critical behavior of systems with many absorbing states,” *Phys. Rev. Lett.* **76**, 451–454 (1996).
- [16] I. Dornic, H. Chaté, and M. A. Muñoz, “Integration of Langevin equations with multiplicative noise and the viability of field theories for absorbing phase transitions,” *Phys. Rev. Lett.* **94**, 100601 (2005).
- [17] M. Henkel, H. Hinrichsen, and S. Lübeck, *Non-equilibrium Phase Transitions Volume 1* (Springer, 2008).
- [18] J. A. Bonachela and M. A. Muñoz, “Self-organization without conservation: true or just apparent scale-invariance?” *Journal of Statistical Mechanics: Theory and Experiment* **2009**, P09009 (2009).
- [19] D. Marković and C. Gros, “Power laws and self-organized criticality in theory and nature,” *Physics Reports* **536**, 41 – 74 (2014).
- [20] D. Forster, *Hydrodynamic Fluctuations, Broken Symmetry, and Correlation Functions* (Taylor & Francis, 1990).
- [21] J. M. Kosterlitz and D. J. Thouless, “Ordering, metastability and phase transitions in two-dimensional systems,” *Journal of Physics C: Solid State Physics* **6**, 1181 (1973).

- [22] B. I. Halperin and D. R. Nelson, “Theory of two-dimensional melting,” [Phys. Rev. Lett. \*\*41\*\*, 121–124 \(1978\)](#).
- [23] U. Frisch, *Turbulence: The Legacy of AN Kolmogorov* (Cambridge University Press, 1995).
- [24] J. Berges, A. Rothkopf, and J. Schmidt, “Nonthermal fixed points: Effective weak coupling for strongly correlated systems far from equilibrium,” [Phys. Rev. Lett. \*\*101\*\*, 041603 \(2008\)](#).
- [25] Z. Hadzibabic, P. Krüger, M. Cheneau, B. Battelier, and J. Dalibard, “Berezinskii-Kosterlitz-Thouless crossover in a trapped atomic gas,” [Nature \(London\) \*\*441\*\*, 1118–1121 \(2006\)](#).
- [26] P. A. Murthy *et al.*, “Observation of the Berezinskii-Kosterlitz-Thouless phase transition in an ultracold Fermi gas,” [Phys. Rev. Lett. \*\*115\*\*, 10401 \(2015\)](#).
- [27] N. Navon, A. L. Gaunt, R. P. Smith, and Z. Hadzibabic, “Emergence of a turbulent cascade in a quantum gas,” [Nature \*\*539\*\*, 72–75 \(2018\)](#).
- [28] M. Prüfer, P. Kunkel, H. Strobel, S. Lannig, D. Linnemann, C.-M. Schmied, J. Berges, T. Gasenzer, and M. K. Oberthaler, “Observation of universal quantum dynamics far from equilibrium,” [arXiv:1805.11881 \(2018\)](#).
- [29] S. Erne, R. Buecker, T. Gasenzer, J. Berges, and J. Schmiedmayer, “Observation of universal dynamics in an isolated one-dimensional Bose gas far from equilibrium,” [arXiv:1805.12310 \(2018\)](#).
- [30] P. Schauß *et al.*, “Crystallization in Ising quantum magnets,” [Science \*\*347\*\*, 1455–1458 \(2015\)](#).
- [31] H. Labuhn *et al.*, “Tunable two-dimensional arrays of single Rydberg atoms for realizing quantum Ising models,” [Nature \*\*534\*\*, 667–670 \(2016\)](#).
- [32] J. Zeiher *et al.*, “Many-body interferometry of a Rydberg-dressed spin lattice,” [Nature Physics \*\*12\*\*, 1095–1099 \(2016\)](#).
- [33] H. Bernien *et al.*, “Probing many-body dynamics on a 51-atom quantum simulator,” [Nature \*\*551\*\*, 579–584 \(2017\)](#).
- [34] J. Zeiher *et al.*, “Coherent many-body spin dynamics in a long-range interacting Ising chain,” [Phys. Rev. X \*\*7\*\*, 041063 \(2017\)](#).
- [35] A. Piñeiro Orioli *et al.*, “Relaxation of an isolated dipolar-interacting Rydberg quantum spin system,” [Phys. Rev. Lett. \*\*120\*\*, 063601 \(2018\)](#).
- [36] I. Lesanovsky and J. P. Garrahan, “Kinetic constraints, hierarchical relaxation, and onset of glassiness in strongly interacting and dissipative Rydberg gases,” [Phys. Rev. Lett. \*\*111\*\*, 215305 \(2013\)](#).

- [37] C. Carr, R. Ritter, C. G. Wade, C. S. Adams, and K. J. Weatherill, “Nonequilibrium phase transition in a dilute Rydberg ensemble,” [Phys. Rev. Lett. \*\*111\*\*, 113901 \(2013\)](#).
- [38] H. Schempp *et al.*, “Full counting statistics of laser excited Rydberg aggregates in a one-dimensional geometry,” [Phys. Rev. Lett. \*\*112\*\*, 13002 \(2014\)](#).
- [39] N. Malossi *et al.*, “Full counting statistics and phase diagram of a dissipative Rydberg gas,” [Phys. Rev. Lett. \*\*113\*\*, 23006 \(2014\)](#).
- [40] A. Urvoy *et al.*, “Strongly correlated growth of Rydberg aggregates in a vapor cell,” [Phys. Rev. Lett. \*\*114\*\*, 203002 \(2015\)](#).
- [41] M. M. Valado *et al.*, “Experimental observation of controllable kinetic constraints in a cold atomic gas,” [Phys. Rev. A \*\*93\*\*, 40701 \(2016\)](#).
- [42] E. A. Goldschmidt *et al.*, “Anomalous broadening in driven dissipative Rydberg systems,” [Phys. Rev. Lett. \*\*116\*\*, 113001 \(2016\)](#).
- [43] C. Simonelli *et al.*, “Seeded excitation avalanches in off-resonantly driven Rydberg gases,” [Journal of Physics B: Atomic, Molecular and Optical Physics \*\*49\*\*, 154002 \(2016\)](#).
- [44] F. Letscher, O. Thomas, T. Niederprüm, M. Fleischhauer, and H. Ott, “Bistability versus metastability in driven dissipative Rydberg gases,” [Phys. Rev. X \*\*7\*\*, 021020 \(2017\)](#).
- [45] R. Gutiérrez *et al.*, “Experimental signatures of an absorbing-state phase transition in an open driven many-body quantum system,” [Phys. Rev. A \*\*96\*\*, 41602 \(2017\)](#).
- [46] C. Ates, T. Pohl, T. Pattard, and J. M. Rost, “Many-body theory of excitation dynamics in an ultracold Rydberg gas,” [Phys. Rev. A \*\*76\*\*, 013413 \(2007\)](#).
- [47] M. Marcuzzi, J. Schick, B. Olmos, and I. Lesanovsky, “Effective dynamics of strongly dissipative Rydberg gases,” [J. Phys. A: Mathematical and Theoretical \*\*47\*\*, 482001 \(2014\)](#).
- [48] M. Marcuzzi, M. Buchhold, S. Diehl, and I. Lesanovsky, “Absorbing state phase transition with competing quantum and classical fluctuations,” [Phys. Rev. Lett. \*\*116\*\*, 245701 \(2016\)](#).
- [49] M. Buchhold, B. Everest, M. Marcuzzi, I. Lesanovsky, and S. Diehl, “Nonequilibrium effective field theory for absorbing state phase transitions in driven open quantum spin systems,” [Phys. Rev. B \*\*95\*\*, 014308 \(2017\)](#).
- [50] C. Pérez-Espigares, M. Marcuzzi, R. Gutiérrez, and I. Lesanovsky, “Epidemic dynamics in open quantum spin systems,” [Phys. Rev. Lett. \*\*119\*\*, 140401 \(2017\)](#).
- [51] G. R. Dennis, J. J. Hope, and M. T. Johnsson, “XMDS2: Fast, scalable simulation of coupled stochastic partial differential equations,” [Comput. Phys. Commun \*\*184\*\*, 201–208 \(2013\)](#).